REPUBLIC OF AZERBAIJAN

On the right of the manuscript

ABSTRACT

of the dissertation for the degree of Doctor of Philosophy

Effect of Gamma Irradiation and Annealing on the Structural Properties of TiN Nanocrystals

Speciality: 2225.01 – Radiation materials science

Field of science: Physics

Applicant: Afsun Sakhavat Abiyev

BAKU – 2025

The work was performed at the "Radiation Physics of Disordered Solids" Laboratory of the Institute of Radiation Problems of the Ministry of Science and Education of the Republic of Azerbaijan.

Scientific supervisor: Doctor of Physical Sciences, prof.
Elchin Mammadali Huseynov

Official opponents: Corresponding Member ANAS, Prof.
Oktay Kazım Qasımov

Doctor of Physical Sciences, Assoc. Prof.
Huseynagha İbrahim Huseynov

Doctor of Physical Sciences, prof.
Famin Tahir Salmanov

Dissertation Council FD 1.21 of the Supreme Attestation Commission under the President of the Republic of Azerbaijan, operating at the Institute of Radiation Problems of the Ministry of Science and Education of the Republic of Azerbaijan

Chairman of the
Dissertation Council: Corresponding Member of ANAS, Prof.
Ogtay Abil Samedov

Scientific Secretary of the
Dissertation Council: PhD in Physics, Assoc. Prof.
Gunel Talat Imanova

Chairman of the
Scientific Seminar: Doctor of Physical and Mathematical Sciences, Prof.
Rahim Salim Madatov

GENERAL DESCRIPTION OF WORK

Relevance and development of the topic. Among refractory nitrides, TiN has gained particular importance in recent years, both from a fundamental and technological perspective. Its stability at high temperatures and chemical resistance make it a promising material for energy systems, micro- and nanoelectronics, as well as protective coating technologies. Nevertheless, real nanocrystalline systems used in industry are not ideal. They are subjected to the influence of defects formed both during the synthesis process and those induced by gamma irradiation and thermal effects during operation. It is precisely this defect architecture that, by altering the lattice parameters, crystallite size, internal microstrain, and surface chemistry, decisively shapes the mechanical strength and electrical–thermal properties of TiN.[1]

The sequential investigation of the effects of gamma irradiation and annealing is essential for understanding how this defect architecture is formed, in which temperature windows it is recovered, and how the functional properties are consequently tuned. Such knowledge enables the design of TiN-based coatings to meet the requirements of radiation and corrosion resistance in nuclear engineering and high-temperature stability in optoelectronics. Moreover, it provides a scientific basis for improving the reliability, longevity, and performance of the material in its various fields of application.

From an applied perspective, TiN is a promising protective coating material for nuclear energy systems and high-temperature components. Its high hardness and chemical stability ensure its durability in reactor environments. The large surface area introduced by the nanoscale strongly couples TiN's reactivity and surface chemistry with the surrounding gaseous atmosphere. This highlights the importance of understanding how processes such as oxidation and oxynitride formation are controlled by irradiation dose and temperature.

[1] Akhtanova, G. [et al.] Electron Irradiation-Induced Degradation of TiN Thin Films on Quartz and Sapphire Substrates / // *ACS Omega*, – 2024, 9, 1, – 925–933.

Accordingly, the key questions of the dissertation are formulated as follows - (1) which defects induced by gamma irradiation cause the most significant damage to the TiN lattice and grain boundaries, (2) how annealing influences defect recombination, (3) how the structural and atomic-scale signatures of these changes correlate with XRD and Raman indicators, and (4) how the thermal events observed by thermal analysis complement these results.

Object and subject of research. The TiN compound used in the study was obtained in powder form. It is a black titanium nitride nanocrystal with a density of 5.22 g/cm³, a purity level of 99.2%, a specific surface area (SSA) of 50–80 m²/g, an average particle size (APS) of 20 nm, a cubic crystal structure, and a melting point of 2950 °C (US Research Nanomaterials, LLC, Houston, USA).

Goals and objectives of the research. The aim of this study is to investigate the structural properties of TiN nanocrystals — including lattice parameters, crystallite size, microstrain, defect formation, and surface oxidation dynamics — under the influence of gamma irradiation and annealing over a wide range of doses and temperatures.

To achieve the stated goal, the following tasks were carried out:

- Irradiation of TiN nanocrystals with gamma rays at doses of 50,200, 900, and 3500 kGy using a Co-60 source
- Carrying out annealing of irradiated and non-irradiated samples in vacuum (10^{-9} Torr) at 1173 K for 9 hours
- Determining lattice parameters, phase composition, and crystallite sizes after irradiation and annealing based on X-ray diffraction results using Rietveld, Scherrer, and Williamson–Hall approaches – determination of microstrain and dislocation density
- Quantitative evaluation of defect formation using PALS/DBAS methods, extraction of depth distribution according to energy-dependence profiles of S and W parameters
- Investigation of the degree of disorder, stress relaxation, and local chemical changes using Raman spectroscopy by monitoring the position and width of vibrational modes

- Detection of the effect of irradiation–annealing sequence on thermal events (relaxation, onset of oxidation, etc.) by DSC/TGA (as well as Cp) measurements and determination of energetic parameters
- Establishing the dependence between structural parameters (a, V, average crystallite size, microstrain, dislocation density) and irradiation dose/thermal regime, as well as evaluation of surface oxidation dynamics
- Modeling the obtained PALS results using MIKA (two-component DFT) software and refinement of defect identification
- Finally, by integrating the results, clarification of the gamma-irradiation → thermal recovery mechanism for TiN nanocrystals and providing recommendations for their fields of application

Investigation methods: High-phase-purity TiN nanopowders were prepared for the investigation, and the initial phase and structure verification were carried out using X-ray diffraction (XRD) and Raman spectroscopy.

Gamma irradiation was performed in a γ-irradiation facility with a Co-60 source. The main γ-lines were 1.17 and 1.33 MeV, and the applied irradiation doses were 50 kGy, 200 kGy, 900 kGy, and 3.5 MGy. The nanocrystal samples were placed in quartz ampoules, and the field was homogenized by ensuring symmetrical distribution in the chamber and equal sample–source distance. The source block is kept in a water pool under normal conditions, and when activated, the Co-60 rods arranged circumferentially in the cassette–tube system are lifted. The sample dimensions and positioning were selected to minimize dose differences arising from geometry.

After irradiation, annealing was carried out under the same pre-defined regime: 1173 K for 9 hours in ~10^{-9} Torr vacuum, with a heating/cooling rate of 5 °C/min. This stage aimed to evaluate the recombination of radiation-induced vacancies, clusters, and intergranular voids, the relaxation of microstrain, and the possible formation of surface oxide layers (TiO_2 rutile).

Phase composition and crystal structure were measured by XRD (Bragg–Brentano θ–2θ geometry, Cu Kα, λ = 1.5406 Å). Instrumental broadening was subtracted using a LaB_6 standard, and Rietveld refinement of the spectrums was performed using the

FullProf package, optimizing the lattice parameter a, unit cell volume V, as well as profile and background parameters. The average crystallite size was estimated using the Scherrer equation, microstrain was evaluated by the Williamson–Hall approach, and dislocation density was calculated using the corresponding expressions; the amorphous phase fraction was quantified based on the integral distribution of peak areas.

For the quantitative analysis of the defect architecture, two complementary methods of positron annihilation spectroscopy were employed. In positron annihilation lifetime spectroscopy (PALS), a ^{22}Na source was encapsulated between Ti foils, and a coincidence setup with two BaF_2 detectors was used, providing a time resolution of ~250 ps; 1274 keV photons were recorded as the "start" signal and 511 keV photons as the "stop" signal. The spectra were processed using multicomponent fitting in the LT9 software package.

Doppler broadening (DBAS) measurements were performed in $\sim 10^{-9}$ Torr vacuum using an HPGe detector. The positron implantation energy was varied in the range of 0–35 keV, and energy-dependent profiles of the S and W parameters were obtained.

The vibrational structure of the crystal lattice and Raman modes were investigated using Raman spectroscopy. Measurements were performed on a high-dispersion laboratory platform equipped with a confocal microscope. Among the available laser wavelengths (473 nm, 532 nm, 633 nm, and 785 nm), the wavelength that minimized local heating in the sample was selected. The laser power was kept below a few milliwatts to further reduce local heating, and the focus diameter was adjusted to ~1 μm. The spectral resolution was ± 0.5 cm^{-1}, and spectra were collected from different surface points of each sample to perform mapping. The obtained Raman lines were fitted with Lorentzian profiles, and information on symmetry, bond strength, and degree of disorder was extracted based on the peak position ($\Delta\nu$), FWHM, and integral intensities.

To monitor thermal events (relaxation, onset of oxidation, etc.), differential scanning calorimetry, differential thermal analysis, and thermogravimetry were employed. Measurements were carried

out in the temperature range of 300–1223 K, with the heating rate selected according to the purpose of each experiment.

Based on the experimental results, calculations were performed using MIKA modeling to refine defect identification. Considering electron–positron interactions, the annihilation rate and lifetime were calculated, and the τ values for various defect configurations were compared with PALS components, enabling the identification of monovacancies as well as cluster types.

All stages were organized in the sequence "irradiation → annealing → analytical measurements → modeling," and measurements performed on the same sets of samples were planned to complement one another.

The main provisions submitted for defense:

- Determination of the stability of the main B1 (NaCl-type) phase, phase transitions, and dose-dependent shifts of Bragg maxima in TiN nanocrystals within the gamma irradiation dose range of 50–3500 kGy.
- Identification of changes in lattice parameter (a), unit cell volume (V), average crystallite size, microstrain, and dislocation density caused by irradiation, based on Rietveld, Scherrer, and Williamson–Hall analyses.
- Demonstration of changes in average crystallite size, crystallinity, and microstrain during the post-irradiation annealing stage, as well as detection of the formation of weak surface-oriented oxide traces.
- Revealing the dose-dependent variation of τ_1 and τ_2 components in PAS results, thereby indicating changes in the size and composition of defects.
- Recording dose-dependent shifts in the position and peaks of the main modes obtained by Raman (combined light scattering) spectroscopy.
- Using DSC/TGA/DTA measurements to clarify the onset of new phase formation (surface processes) in TiN nanocrystals under thermal influence and to track the temperature-driven evolution of radiation-induced modifications after high-dose gamma irradiation.

- Identification of defect types using calculations based on PALS lifetime components performed in the MIKA program.

Scientific novelty of the research. For the first time, the present dissertation has established that:

For the first time:

1. It was established that within the gamma irradiation range of 50–3500 kGy, the main B1 (NaCl-type) phase in TiN nanocrystals remains stable; dose-dependent shifts of Bragg maxima were observed in X-ray diffraction patterns, along with a reduction in lattice parameters and a decrease in long-range order.
2. Post-irradiation annealing (1173 K, 9 h) was shown to improve crystallinity, increase crystallite size, and reduce microstrain; rutile TiO_2 was detected, and the fraction of the oxide phase was quantitatively evaluated.
3. Average crystallite size, microstrain, and dislocation density were quantitatively determined using Scherrer and Williamson–Hall approaches.
4. Using positron annihilation lifetime spectroscopy (PALS), dose-dependent changes were recorded in the lifetimes and intensities of short- and long-lived components, and changes in defect size and composition were quantitatively substantiated.
5. Doppler broadening annihilation spectroscopy (DBAS) revealed an increased contribution of annihilation in open-volume defects; based on energy-dependent profiles, information on the distribution of these defects from the surface toward the bulk was obtained.
6. Systematic, irradiation-sensitive changes in the position and FWHM of the main modes were identified by Raman (combined light scattering) spectroscopy, and these changes were explained by stress relaxation and modifications in the local bonding environment.
7. A quantitative correlation between PALS lifetime components and specific defect types was demonstrated using the MIKA program, thus providing theoretical validation of the experimental indicators.
8. DSC, TGA, and DTA measurements revealed additional thermal events and mass changes during the heating of irradiated TiN

nanocrystals, particularly in the 740–800 K range, and these phenomena were attributed to structural reorganization and surface oxidation.

The theoretical and practical significance of the research: The results obtained in this dissertation demonstrate that the long-term operational stability of TiN-based materials in reactor environments (e.g., as protective layers on fuel claddings and structural elements) can be controlled through specific parameters: lattice parameter, crystallite size, microstrain, and defect formation can be tuned by the sequence of gamma irradiation and subsequent annealing, while the formation of thin TiO_2 traces on the surface can be kept under control. This enables the rational selection of materials and process regimes to achieve practical effects such as reduced local wear and corrosion risks.

At the same time, the advantages of TiN — such as hardness, chemical resistance, and high-temperature stability — can be tailored based on the structural properties established in this work for targeted applications in diffusion barriers and sensor platforms of MEMS/NEMS devices.

Approbation and application:

The scientific results obtained in the dissertation were presented at several international and local scientific events in accordance with the different directions of the research and were brought to scientific discussions. The results of the studies were reported at various conferences and were evaluated by specialists.

- ✓ Abiyev A. S., Huseynov E.M. The Effects of Gamma Irradiationon TiN Nanocrystals // Курчатовский институт “OpenScience” - Санкт-Петербург, Россия: -15-17 november - 2023. – p. 57
- ✓ Abiyev A. S., Səmədov S., Hüseynov E., Sidorin A.A., Orlov O. Qamma şüaların təsirinə məruz qalmış nanoölçülü TiN kristallarında defekt əmələgəlmə mexanizminin tədqiqi // Radiasiya təhlükəsizliyi problemləri: Regional aspektlər, Azərbaycan, Naxçıvan: – 18–19 oktyabr, – 2023, –p.95.
- ✓ Abiyev A. S., Turchenko V. A., Huseynov E. M., Changes in crystallinity properties of TiN nanoparticles after gamma rays and

long – term heating process // II International Conference Fundamental and Applied Problems of Semiconductor Physics, Micro- and Nanoelectronics - Tashkent, Uzbekistan: - 2023, - p. 261-262.

- ✓ Abiyev A. S., Samadov S. F., Huseynov E. M. Defect formation analysis in gamma-irradiated titanium nitride nanocrystals:predictions from positron annhilation studies // Metal və ərintilər fizikasının aktual problemləri" Respublika Elmi-Praktiki Konfransı - Azərbaycan. -2025, -p.146-148.
- ✓ Abiyev A. S., Huseynov E. M. Characterization of Thermal Effects on TiN Nanocrystals after Gamma Irradiation // Молодежная Школа по физике конденсированного состояния (Школа ФКС-2025) - Рощино, Ленинградская область: - 24 - 28 марта 2025, p.134.

Publications: The main content and scientific results of the dissertation have been reflected in 6 articles published in international journals and 5 abstracts published in the proceedings of international scientific conferences. In total, the main results of the dissertation have been published in 11 scientific works.

The name of the organization where the dissertation work was performed: The experiments conducted within the framework of the dissertation were performed at the Institute of Radiation Problems of the Ministry of Science and Education of the Republic of Azerbaijan.

Personal attendance of the author: The main scientific results presented in the dissertation are the outcome of the applicant's own scientific work. The applicant substantiated the relevance of the research topic, carried out a comprehensive investigation of the structural, thermal, and surface properties of nanocrystalline TiN samples subjected to gamma irradiation, and systematized the obtained results, providing their scientific interpretation. In addition, the applicant was directly involved in presenting the research results at scientific conferences and in the preparation of publications.

The total volume of the dissertation with a character including a separate volume of the structural units of the

dissertation. The dissertation consists of an introduction, five chapters, a conclusion, a list of references, and abbreviations, covering a total of 148 pages. The main text (excluding figures, tables, and the reference list) comprises 173,011 characters in total. The distribution of characters across the sections is as follows: Introduction – 27,845; Chapter I – 46,316; Chapter II – 28,925; Chapter III – 24,235; Chapter IV –44,343; Conclusion – 1,347. The research work contains 37 figures and 8 tables, and the list of references includes 216 sources.

THE CONTENT OF THE DISSERTATION

In the **Introduction,** the relevance of the topic — the importance of gamma irradiation and annealing effects on the structural properties of TiN nanocrystals in materials science and technology — is substantiated, the purpose of the research, its scientific novelty, and practical significance are presented, the main provisions submitted for defense are listed, and information is provided on the scope of approbation and published works. A brief summary of the content of the dissertation by chapters is also presented**.**

In the **first chapter,** data on the synthesis of TiN nanomaterials, their crystal-chemical structure and phase stability, microstructural evolution under the influence of temperature, as well as radiation defects generated by ionizing radiation (gamma, electron, and ion beams, in the context of the literature) are collected and analyzed. The main objective of this chapter is to summarize the results of studies presented in the literature on TiN nanocrystals subjected to ionizing radiation and to establish the scientific basis for the measurements carried out in this dissertation.

Based on the reviewed sources, the relevance of the topic is substantiated — specifically, the structural stability of TiN under high-temperature and radiation loads, the formation and control of defect architecture, and the conditions for the appearance of surface oxidation traces — and the necessity of continuing scientific research in this direction is emphasized.

In addition, detailed information is provided on the role of processes used in coating and semiconductor technologies (reactive gas-phase deposition, thermal stabilization, and ion implantation, as discussed in the literature) in shaping the initial microstructure, texture, and defect distribution of TiN. The analysis shows that the quantitative description of the combined effect of gamma irradiation and annealing on the structural properties of nanocrystalline TiN (lattice parameters, crystallite size, microstrain, and open-volume defects) remains a relatively underexplored area, thereby confirming the scientific and technological significance of the research direction chosen in this dissertation.

In the **second chapter,** the research design is presented as a unified workflow: high-purity TiN nanopowder was prepared, and the initial phase and structural identification were performed by XRD and Raman spectroscopy, confirming the B1 (Fm-3m) cubic phase. The samples were irradiated at room temperature with a Co-60 source at doses of 50, 200, 900 kGy, and 3.5 MGy; field homogeneity and the actual absorbed dose were ensured in advance by dosimetric calibration.

Following irradiation, the same samples were thermally treated at 1173 K for 9 hours in ~10^{-9} Torr vacuum with a heating/cooling rate of 5 K/min, targeting the recombination of radiation-induced defects, relaxation of microstrain, and evaluation of possible surface oxidation. Structural analysis was performed by XRD in Bragg–Brentano geometry with Cu Kα radiation, applying Rietveld refinement; crystallite size and microstrain were determined using the Scherrer and Williamson–Hall approaches, while the amorphous fraction was quantified from the integral distribution of peak areas.

The defect architecture was studied using positron annihilation-based methods: PALS (^{22}Na, ~250 ps resolution) allowed separation of short- and long-lived components, while DBAS (0–35 keV) provided energy-dependent S/W parameter profiles, revealing depth distributions from the surface to the bulk. The vibrational properties of atomic dynamics were obtained by Raman spectroscopy. Thermal events in the range of 15–1000 °C

were synchronously monitored by DSC/TGA/DTA, and energetic signatures of relaxation and surface reactions were determined via heat flow. Finally, the correspondence between PALS lifetime components and specific defect configurations was refined using MIKA two-component calculations, thus completing the "irradiation → annealing → characterization → simulation" sequence on the same set of samples.

In the **third chapter** of the dissertation, the crystallographic structure of TiN nanocrystals after exposure to gamma irradiation (50 kGy, 200 kGy, 900 kGy, and 3.5 MGy) was systematically studied by X-ray diffraction (XRD)[2].

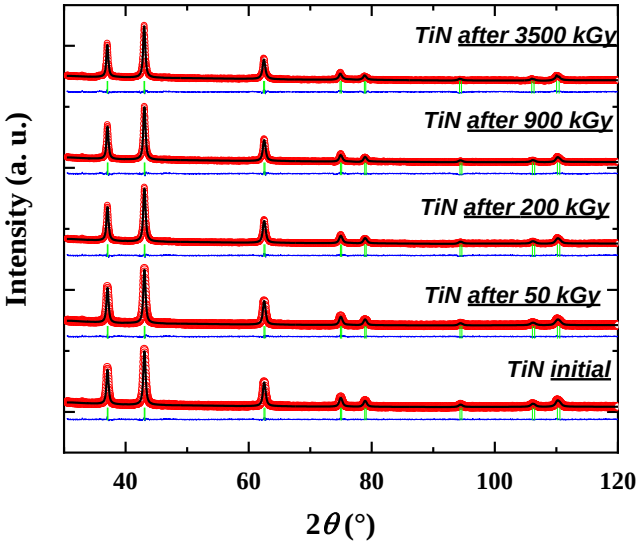

Figure 1. X-ray diffraction patterns of unirradiated and gamma-irradiated TiN nanoparticles at various doses. The red dots represent the experimental data, the black lines correspond to the theoretical fit, the blue lines show the difference between experimental and calculated profiles, and the green vertical lines indicate the Bragg reflection positions.

[2] Brager, A. An X-ray examination of titanium nitride. // III Acta Physicochimica (USSR), – 1939, 9, – p. 617-632.

The spectrums showed peaks characteristic of the B1 (NaCl-type, Fm-3m) cubic phase (figure 1.), which were indexed according to the (111), (200), (220), (311), (222), (400), (331), and (420) plane families. In the unirradiated sample, the main (111) maximum was recorded at $2\theta \approx 43.09°$, and the corresponding interplanar spacing was calculated as $d \approx 2.122$ Å. Based on Rietveld refinement, the initial lattice parameter was determined as $a \approx 4.2444$ Å, and the unit cell volume as $V \approx 76.46$ Å^3.

Long-term irradiation (highest dose ~3.5 MGy) did not disrupt the phase stability: the salt-type cubic structure of TiN was preserved at all dose levels, with no new phase formation or phase transitions detected. Nevertheless, small but systematic shifts of the peaks and an increase in line broadening were observed. The shift of the peaks toward higher angles along the abscissa indicates a reduction of the lattice parameter. The general trend is as follows: as the dose increases, the lattice parameter slightly decreases, and the unit cell volume correspondingly becomes slightly smaller

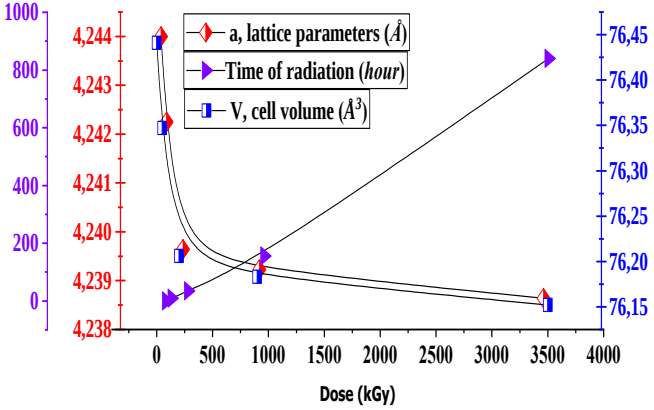

Figure 2. Dependence of the lattice parameters and unit cell volume of TiN nanoparticles on the irradiation dose

This change is most pronounced during the transition from low to medium doses, while at higher doses it continues with a "saturated" weak trend (figure 2.).

The variation of diffraction peak positions and FWHM makes it possible to calculate how the nanocrystallite size and microstrain change with dose. According to the Scherrer approach, the average crystallite size in the unirradiated state is around ~20 nm and decreases to ~18.5 nm as the dose increases (overall reduction ≈ 7–8%). The increase of the amorphous fraction area in the background of the spectra with increasing dose indicates a reduction of long-range order. In this case, the amorphous fraction rises approximately in the sequence 0.3% → 0.5% → 1.2% → 2.5%.[3]

The evaluation of microstrain and dislocation density showed that irradiation leads to an increase in internal stresses: the microstrain ε rises from ~3.18×10^{-3} to ~3.51×10^{-3}, and the dislocation line density correspondingly increases. This growth corresponds to the formation of new defect centers and stress fields in the crystal lattice, which in turn contribute to peak broadening. These changes, occurring under conditions of phase stability, manifest primarily as structural refinements — namely, slight "compression" of the lattice, reduction in average particle size, and enrichment of the defect architecture.

The decrease in crystallite size and the increase in amorphous fraction are associated not only with radiation damage but also with the dynamics of surface chemistry. During irradiation, the possible decomposition of adsorbed H_2O/OH groups and Ti–OH surface layers, the release of volatile reaction products (e.g., NH_3, H_2), and the resulting local reorganization processes are indicated. The observation of rapid changes at low doses and a relatively weaker trend at higher doses is consistent with the fact that the majority of these "loosely bound" surface layers are already removed at low–medium doses.

To monitor the size and depth of the defect architecture created by gamma irradiation, two complementary positron annihilation spectroscopy techniques were employed: positron annihilation lifetime spectroscopy (PALS) and Doppler broadening

[3] Mirzayev N. M. Determination of amorphization oxide layers, mobilization and functional groups on ZrC nanocrystals under high gamma irradiation // *Vacuum* - 238, 114215, 2025.

annihilation spectroscopy (DBAS). These methods allow sensitive identification of positron trapping and annihilation processes at open-volume centers (vacancies, clusters, intergranular voids).

Figure 3 shows that PALS measurements for TiN nanocrystals reveal two main components: a short-lived τ_1 (trapping at monovacancy-sized or small centers) and a long-lived τ_2 (associated with large voids/vacancy clusters).

As the irradiation dose increases, both τ_1 and its intensity (I_1) gradually rise, indicating either an increase in the number of $1V_{ti}$-type centers or their partial transformation into small complexes such as $1V_{ti}+1V_n$, thereby enhancing their effective trapping capacity.[4] In parallel, τ_2 also increases, but the intensity of the long-lived component (I_2) decreases, which corresponds to a scenario where large vacancy clusters grow in size but decrease in number.

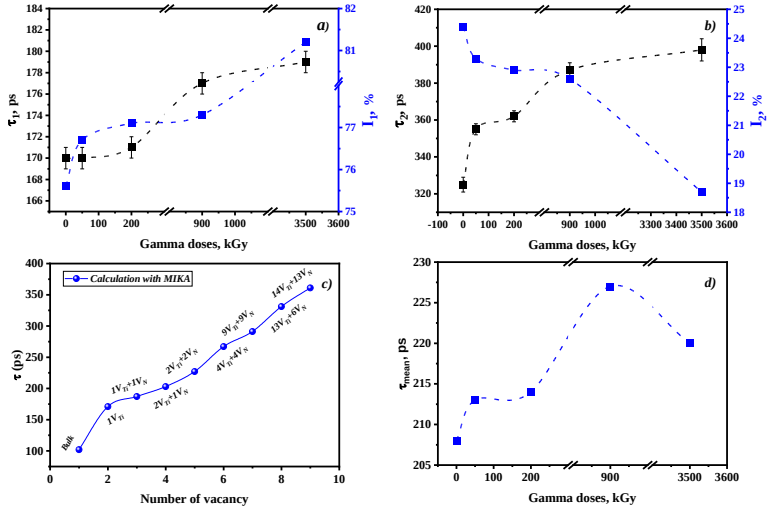

Figure 3. PAS results for TiN nanocrystals. The plotted variables are: a) dependence of τ_1 and I_1 on gamma dose; b) dependence of τ_2 and I_2 on gamma dose; c) calculated variation of lifetime with increasing vacancy cluster volume; d) dependence of τmean and τb on gamma dose.

[4] Bordulev, I. et.al. Positron Annihilation Spectroscopy Complex for Structural Defect Analysis in Metal–Hydrogen Systems // *Mater.*, – 2022, 15, 1823, – 15 p.

The calculated typical values indicate that τ_1 for monovacancies is around ~170 ps, while τ_2 for large cluster configurations is at the level of ~360 ps; the experimental lifetime components agree well with these ranges.

Application of the two-state trapping model shows that, as the dose increases, indicators sensitive to void size tend to grow (increase of the τ_2–τb difference), whereas in some samples a decrease in the effective trapping rate (k_d) can be observed. This is not a contradiction: the coalescence of large clusters can reduce the effective number of traps while increasing the volume of the existing ones. As a result, the average size increases and the number decreases — leading to an increase in τ_2 and a decrease in I_2. The calculated typical values indicate that τ_1 for monovacancies is around ~170 ps, while τ_2 for large cluster configurations is at the level of ~360 ps, the experimental lifetime components agree well with these ranges.[5]

Application of the two-state trapping model shows that, as the dose increases, indicators sensitive to void size tend to grow (increase of the τ_2–τb difference), whereas in some samples a decrease in the effective trapping rate (k_d) can be observed. This is not a contradiction: the coalescence of large clusters can reduce the effective number of traps while increasing the volume of the existing ones. As a result, the average size increases and the number decreases — leading to an increase in τ_2 and a decrease in I_2. After the impact of gamma quanta, the positron annihilation depth was studied using variable-energy positron beams.

Based on the results shown in Figure 4 a, it is observed that for both the initial (unirradiated) and irradiated samples, as the annihilation depth increases, the S parameter decreases. The S parameter can be interpreted as an indicator characterizing the scale of bulk-type defects in the material. In titanium nitride (TiN) crystallites, an increase in vacancy volume is recorded as a result of gamma irradiation.

[5] Brunner, J., Perry, A.J. Positron lifetime study of vacancy defects in non-stoichiometric TiNx and TiCx films // *Thin Solid Films*, – 1988, 163, – p. 49-54.

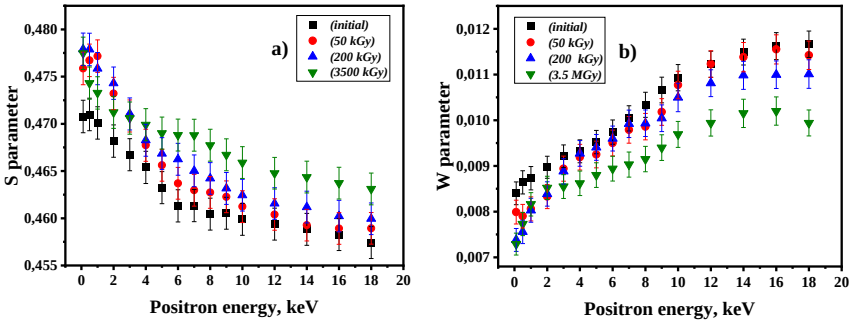

Figure 4. Dose-dependent variation curves of the S (a) and W (b) parameters as a function of depth (energy) for TiN nanocrystals.

On the other hand, as the gamma dose increases, the value of the S parameter rises, which indicates an increase in defect concentration.[6] From 10 keV onward, a homogeneous distribution of defects with depth is observed. The S parameter characterizes positron annihilation with valence electrons, while the W parameter characterizes annihilation with core electrons. In the absence of positronium formation, the S and W parameters serve as "mirror-like" indicators of defect formation in the material. In a defect-free crystal structure (when the S parameter decreases), annihilation with core electrons increases while annihilation with valence electrons decreases; conversely, in the presence of defects, annihilation with valence electrons becomes stronger and with core electrons weaker.

In our work, it is clearly observed that as the irradiation dose increases, the S parameter rises with positron energy, while the W parameter decreases. Therefore, it is expected that the depth profiles of the S and W parameters should appear as mirror images of one another.

[6] Brusa, R.S. G.P.Karwasz, N.Tiengo [et al.]. Formation of vacancy clusters and cavities in He-implanted silicon studied by slow-positron annihilation spectroscopy // *Phys. Rev. B.*, – 2000, 61(15), – p. 10154–10166.

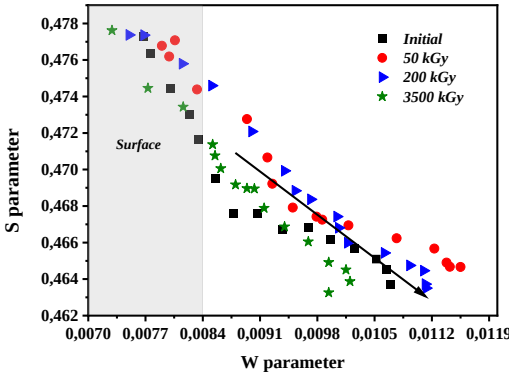

Figure 5. S–W diagram for TiN nanocrystals: the points that deviate from the straight line indicate the presence of multicomponent defects.

In Figure 5, the fact that the points in the S–W correlation diagram do not lie along a single line indicates that the defect mechanism is not limited to a single type of center, but rather reflects the coexistence of different types of vacancy configurations (mono-/divacancies, mixed VTi+VN complexes, and intergranular voids).

In the DBAS profiles, the "shift" of near-surface signals toward greater depths in the 0–7 keV interval with increasing dose strengthens the assumption of diffusion of contaminant species (O, OH) into intergranular regions.[7]

Overall, TiN particles remain structurally and functionally stable up to doses of 3.5 MGy. The observed changes are mainly limited to the reorganization of defect architecture and minor modifications of surface chemistry.

Raman spectroscopy was used to monitor the atomic dynamics of TiN nanocrystals, and four main modes were resolved in the range ν = 100–600 cm^{-1}. Mathematical processing of the spectra was performed using a mixture of Lorentz–Gauss (pseudo-Voigt) profiles, and parametric fitting was carried out for the peak position (ν), FWHM, and integral intensities. In the unirradiated sample, the

[7] Bull, S.J., Evans, P.C., Saleh, A.S. Positron annihilation studies of defects in PVD TiN coatings // *Surface and Coatings Technology*, – 1996, 78(1-3), – p. 42-49.

mode centers were determined to be approximately $\nu_1 \approx 152$ cm^{-1}, $\nu_2 \approx 246$ cm^{-1}, $\nu_3 \approx 359$ cm^{-1}, and $\nu_4 \approx 500$ cm^{-1}. Compared to the reported values for thin films, these positions are slightly lower, which is explained by the stronger role of surface effects, size confinement, and localized stresses in nanopowders.

The TiN compound possesses an ideal cubic structure. Trivalent Ti atoms occupy the lattice sites of the crystal with atomic coordinates x = 0, y = 0, z = 0. Trivalent N atoms, which form covalent bonds with Ti atoms, are distributed throughout the crystal volume and occupy the coordinates x = 0.5, y = 0.5, z = 0.5. In a structure with lattice parameters a = b = c ≈ 4 Å, the Ti–N distance is dTi–N = 2.1 Å, while the Ti–Ti distance is dTi–Ti = 3 Å. Along the unit cell, Ti and N atoms alternate according to the NaCl model. It is known that in the periodic table, N atoms are in the 7th position, whereas Ti atoms are in the 22nd position. However, in the trivalent state, the ionic radius of N atoms becomes larger than that of Ti atoms: $R_{N^{3-}}$ = 1.72 Å, $R_{Ti^{3+}}$ = 0.66 Å. This is because the three electrons in the outer shell of Ti atoms are transferred to N atoms. Therefore, in the trivalent state, the ionic radius of N atoms becomes larger, and the N atoms surrounding Ti atoms form a TiN_6 octahedral system, which is sufficiently resistant to external influences.

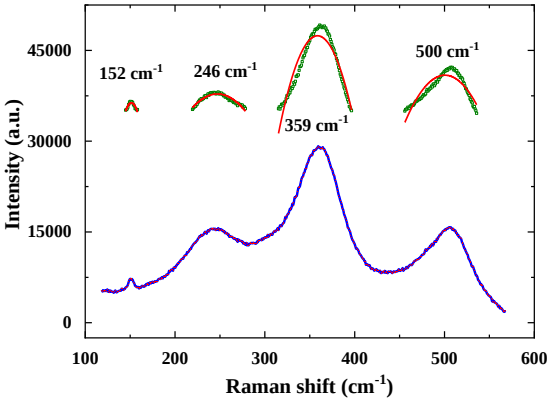

Figure 6. Raman spectrum of TiN nanoparticles: decomposition of four main components in the range of 100–600 cm^{-1}.

The crystal structure of TiN corresponds to the NaCl-type B1 phase: Ti atoms occupy the cube corners, while N atoms are located at the cube center; the lattice parameter is ~4 Å, the Ti–N bond length is approximately 2.1 Å, and the Ti–Ti distance is ~3.0 Å. The formation of TiN_6 octahedra determines the symmetry and stiffness of the vibrational modes (figure 6.).[8] Raman spectra were compared as a function of irradiation dose. In the range from 50 kGy to 3.5 MGy, the phase stability is preserved, and all the main modes remain present; this result is in full agreement with the XRD evidence. The positions of the modes exhibit systematic but directionally different evolution with dose: ν_1 remains practically unchanged, ν_2 slightly decreases, while ν_3 and ν_4 increase. The calculated trends can be estimated as $k_1 \approx +5.7\times10^{-4}$ $(cm\cdot kGy)^{-1}$, $k_2 \approx -2.5\times10^{-3}$ $(cm\cdot kGy)^{-1}$, $k_3 \approx +6\times10^{-3}$ $(cm\cdot kGy)^{-1}$, and $k_4 \approx +3.4\times10^{-3}$ $(cm\cdot kGy)^{-1}$, respectively.

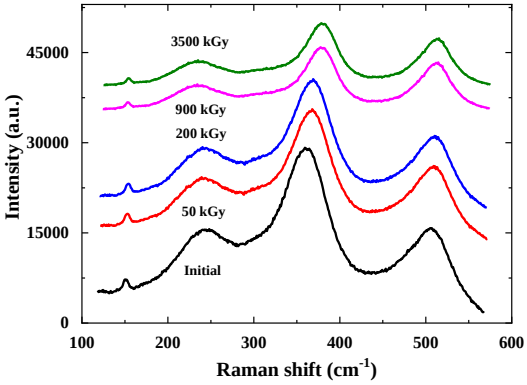

Figure 7. Shift characteristics of the modes of TiN nanoparticles under different irradiation doses obtained by the Raman spectroscopy.

This behavior of vibrational frequencies is associated with changes in local bond lengths and force constants. The increase in ν_3/ν_4 with dose may indicate enhanced bond stiffness in certain

[8] Christensen, A. A. [et al.]A Neutron Diffraction Investigation on Single Crystals of Titanium Carbide, Titanium Nitride, and Zirconium Nitride / // *Acta Chemica Scandinavica*, - 1975, 29a, - p. 563-564.

directions (local compression or defect reconstruction effects), whereas the decrease in ν_2 may reflect bond weakening in other directions (local expansion, breaking of weak bonds, or thermal/radiation-induced decomposition of Ti–(OH) groups).

Due to the large surface-to-bulk ratio in nanocrystals, adsorbed species can easily desorb or undergo reconstruction under irradiation, producing subtle but measurable effects on the vibrational spectrum. As a result, the combined analysis of Raman, XRD, and PALS/DBAS reveals a macrostructurally phase-stable but microstructurally dose-sensitive picture.[9]

In the **fourth chapter** of the dissertation, the results obtained after annealing of gamma-irradiated TiN nanocrystals at 1173 K for 9 hours are presented in Figure 8. Rietveld refinement of the XRD data shows that the B1 (Fm-3m) cubic phase is preserved at all doses; at the same time, traces of TiO_2 (rutile) related to surface oxidation are detected: the peaks at $2\theta \approx 54.33°$ and $56.63°$ are indexed as the (211) and (220) reflections, respectively, and the fraction of the rutile phase is estimated to be approximately 6.4%.

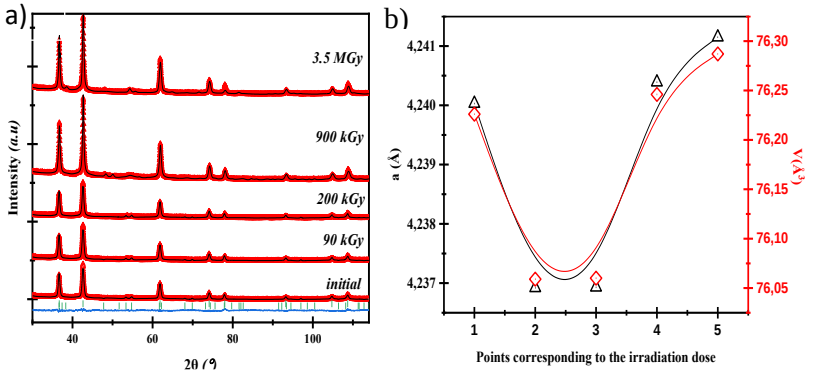

Figure 8. a) X-ray diffraction patterns of TiN nanocrystal samples after annealing b) variation mechanism of lattice parameters obtained from Rietveld refinement.

[9] Das, S. Influence of nitrogen gas over microstructural, vibrational and mechanical properties of CVD Titanium nitride (TiN) thin film coating / S.Das, S.Guha, R.Ghadai [et al.] // *Ceram. Int*., - 2021, 47, - p. 16809–16819.

These findings confirm that the oxidation is localized and occurs as a thin surface layer, while the TiN cubic structure is preserved in the bulk. Comparison of the diffraction peak profiles indicates improved crystallinity after annealing, and Williamson–Hall analysis confirms a reduction in microstrain. Although a slight decrease in the lattice parameter is observed after low-dose irradiation, at higher doses (particularly 900 kGy and 3.5 MGy) the crystallite size grows up to ~50 nm due to defect recombination and reorganization. This correlates with the decrease in dislocation density. The plots of lattice parameter a and unit cell volume V support the proposed mechanism of structural dynamics.[10]

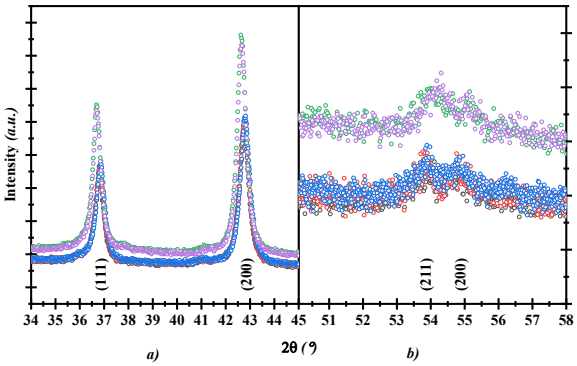

Figure 9. a) XRD profiles of the diffraction peaks indexed as (111) and (200) for TiN nanocrystals after irradiation at various doses followed by annealing at 1173 K, b) Appearance of the TiO_2 phase in irradiated samples after annealing, with peaks indexed as (211) and (220).

In Figure 9 a), the FWHM and intensity of the diffraction peaks for the initial, 90 kGy, and 200 kGy irradiated samples followed by annealing are observed to decrease. This indicates an improvement in crystallinity and simultaneously reflects the influence of the TiO_2 rutile phase. As can be seen from the spectra in Figure 9b, the

[10] Popov, E.P. Slavov L., Demir E. [et al.] Microstructural evolution of TiC nano powders under fast neutron irradiation: A multi-technique analysis // *Vacuum*, - 2023, 215, 112338.

formed oxide phase is largely amorphous. The TiO_2 phase forms at the expense of the TiN phase, and the transition of some particles into the new phase leads to a reduction in intensity.

Changes in the defect architecture were monitored using positron annihilation methods. The PALS spectra are described by two components: a short-lived $\tau_1 \approx 0.155–0.166$ ns (monovacancies and small clusters) and a long-lived $\tau_2 \approx 0.394–0.409$ ns (large open-volume clusters).[11] In the two-state trapping model, the decrease of the kd parameter from 0.720 → 0.709 nm^{-1} indicates a weakening of positron trapping in large voids after annealing.

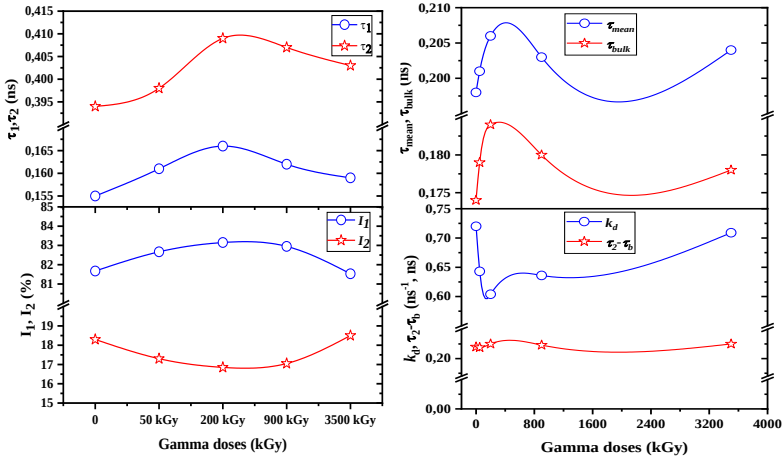

Figure 10. PALS results for TiN nanocrystals irradiated at different absorbed doses and the dose dependence of the positron trapping parameters at 1173 K.

All these effects can be explained by defect recombination and the migration of a portion of defects to the surface or grain boundaries. A visual representation of the results is provided in Figure 10. From the energy dependence of the S parameter obtained from the DBAS measurements presented in Figure 11, surface

[11] Knights, A.P. A.P.Knights, A.S.Saleh, P.C.Rice-Evans et al. Investigation of magnetron-sputtered titanium nitride films using positron annihilation spectroscopy // *Journal of Physics: Condensed Matter*, – 1996, 8(14), – p. 2479-2486.

trapping can be observed at low energies, while above ~14 keV a homogeneous distribution with depth is seen. The fact that the S values in irradiated samples remain higher than those of the initial state indicates the presence of residual vacancy-type centers.[12]

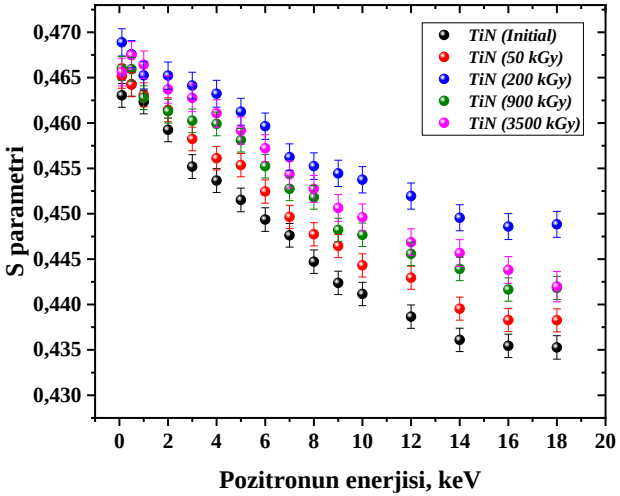

Figure 11. Doppler broadening annihilation curve as a function of positron implantation energy for TiN nanocrystals.

In the thermal analysis section, the DSC/TGA/DTA results complement the structural relaxation and oxidation dynamics: in high-dose samples, weak anomalies are recorded in the range of 740–800 K, which are associated with temperature-driven recombination of radiation-induced defects and local oxidation events. Synchronous analysis of mass change and heat flow shows that oxidation is mainly confined to the surface scale and corresponds to the rutile traces observed in XRD; the TiN cubic structure remains stable as the bulk phase.

Overall conclusion: annealing modifies the defect architecture created by gamma irradiation in a controllable manner — crystallites

[12] Klym, H. H.Klym, I.Karbovnyk, S.Piskunov et al. Positron Annihilation Lifetime Spectroscopy Insight on Free Volume Conversion of Nanostructured MgAl2O4 Ceramics / // *Nanomaterials*, - 2021, 11, 3373, - 11 p.

grow, microstrain and dislocation density decrease, and the surface oxide phase remains thin and limited.[13]

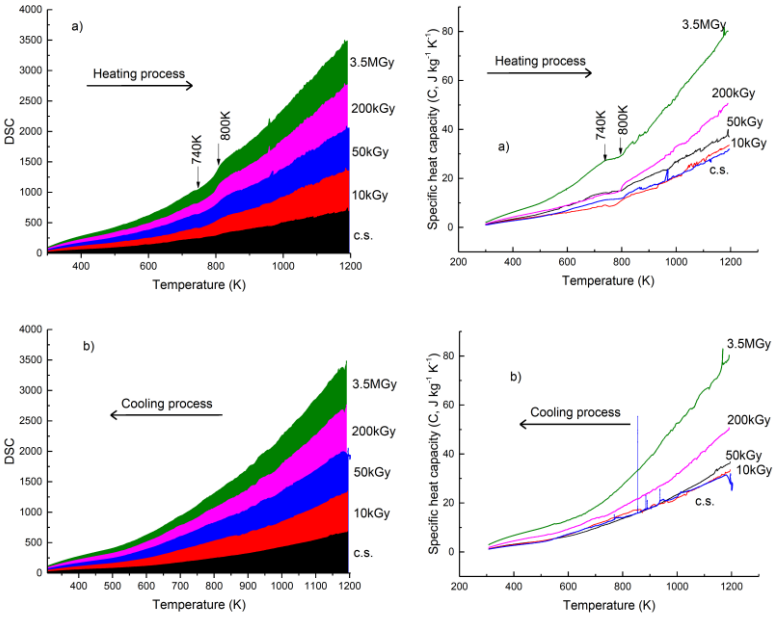

Figure 12. a) DSC curves of TiN nanoparticles irradiated with gamma rays during heating and cooling processes, and b) variation of the temperature-dependent specific heat capacity of TiN nanoparticles as a function of irradiation dose.

Using DSC (differential scanning calorimetry), it is possible to study the thermal behavior of TiN, its energy storage capacity, phase stability, and, additionally, its specific heat capacity based on measurements and thermodynamic modeling.

The experimental approach combines DSC and heat capacity measurements with Gibbs free energy as well as entropy–enthalpy analyses to provide a comprehensive assessment of radiation-induced changes in TiN.

[13] Huseynov, E.M., Naghiyev, T.G. Investigation of thermal parameters of AlN nanoparticles at the different heating rates // *Vacuum*, – 2023, 212, 111990, – p. 10-14.

Figure 13a presents the differential scanning calorimetry (DSC) thermograms of nanocrystalline TiN samples exposed to different gamma irradiation doses (10 kGy, 50 kGy, 200 kGy, and 3.5 MGy) and describes their thermal behavior during heating and cooling processes.

As shown in Figure 13b, during heating, the specific heat capacity of all samples increases with temperature, which is consistent with the expected behavior for solids. However, in the sample irradiated at the highest dose of 3.5 MGy, two distinct anomalies are observed at approximately 740 K and 800 K.[14]

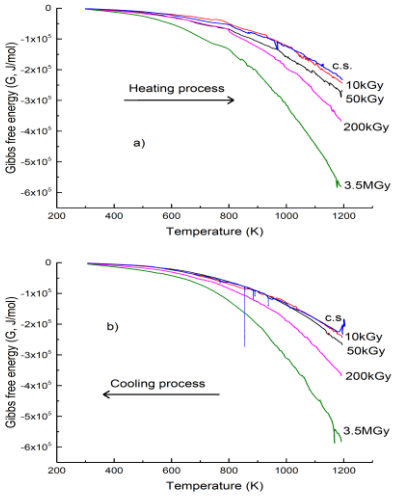

Figure 13. Evolution of Gibbs free energy in gamma-irradiated TiN nanoparticles: analysis of thermodynamic stability.

Figure 13 presents the evolution of Gibbs free energy (G, C/mol) as a function of temperature for nanocrystalline TiN samples exposed to different gamma irradiation doses (10 kGy, 50 kGy, 200

[14] Klimesch, D.S., Ray, A. DTA-TGA evaluations of the CaO–Al2O3–SiO2–H2O system treated hydrothermally // *Thermochimica acta*, – 1999, 334(1-2), – p. 115-122.

kGy, and 3.5 MGy), showing the behavior during both heating and cooling processes.

During the heating stage (Figure 14 a), a gradual decrease in Gibbs energy is observed with increasing temperature for all samples, which corresponds to entropy-driven stabilization as thermal energy is introduced. In the cooling process, the trends of Gibbs energy display a more uniform character compared to heating, with fewer fluctuations.[15]

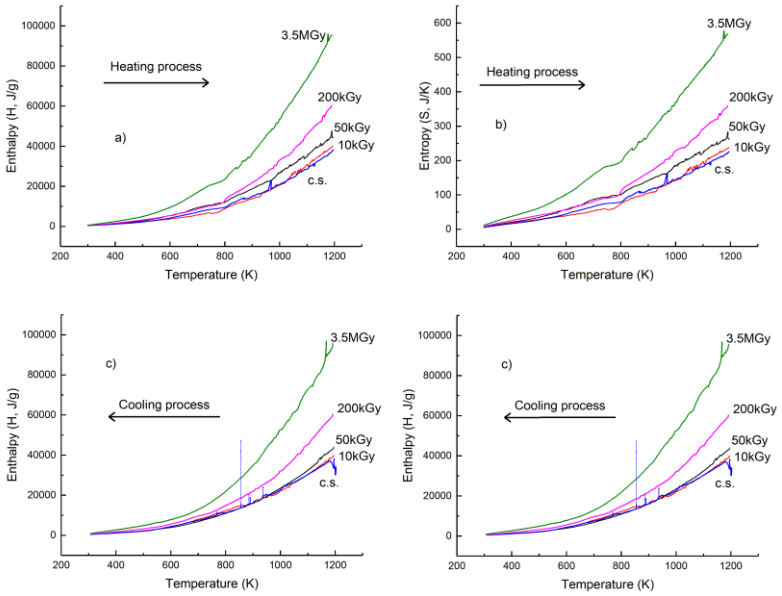

Figure 14. Enthalpy and entropy variations in TiN nanoparticles under gamma irradiation: energy storage and disorder effects.

Figure 14 provides a direct insight into heat energy storage and the evolution of entropy for irradiated TiN. During the heating process (Figure 14a), enthalpy exhibits a temperature-dependent

[15] Huseynov, E.M., et.al. U.S. Thermal parameters investigation of neutron-irradiated nanocrystalline silicon carbide (3C–SiC) using DTA, TGA and DTG methods // *Physica B: Condensed Matter*, – 2020, 577, 411788, – 5 p.

increase consistent with the accumulation of thermal energy. At lower radiation doses (10 kGy, 50 kGy, and 200 kGy), the rate of increase remains relatively constant, indicating that the effect on energy absorption is minimal. However, in the sample irradiated at 3.5 MGy, a noticeable deviation is observed near approximately 740 K and 800 K. The evolution of entropy (Figure 14b) reflects the degree of disorder introduced by irradiation, further reinforcing these findings. At lower irradiation doses, entropy increases smoothly with temperature, indicating the stability of the crystal structure. In contrast, the cooling process (Figure 14c) exhibits a more uniform enthalpy trend, resembling the behavior observed for heat capacity and Gibbs free energy in Figures 13 and 14, respectively.[16]

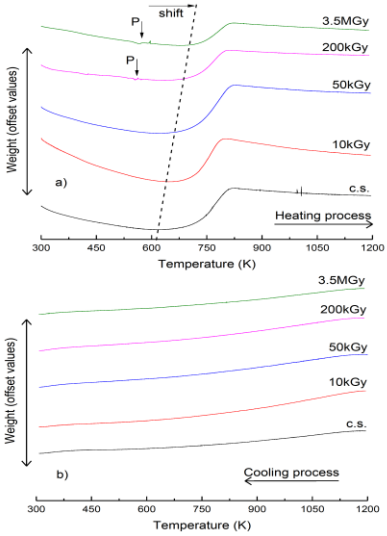

Figure 15. Temperature-dependent mass change of nanocrystalline TiN particles before gamma irradiation (c.s.) and after irradiation at various doses (50 kGy, 200 kGy, 900 kGy, and 3.5 MGy); (a) heating process, (b) cooling process.

[16] Huseynov, E.M., Naghiyev, T.G. Investigation of thermal parameters of AlN nanoparticles at the different heating rates // *Vacuum*, – 2023, 212, 111990, – p. 10-14.

This correspondence indicates that the main radiation-induced transformations occur during heating and are not fully reversible during cooling.

Figure 15a shows the temperature-dependent mass change of nanocrystalline TiN particles before and after gamma irradiation. It is important to note that the experimental results are not dependent on absolute mass values; these values are purely technical and carry no physical significance.

As seen in the figure, the kinetics of mass change differ between the heating and cooling processes (Figures 15a and 15b). During heating, in the temperature range of approximately 300 K < T < 600 K, no significant mass loss is observed (Figure 15a). However, before irradiation, a more pronounced mass loss is recorded, indicating that the surface chemistry of the material plays a decisive role in its thermal response.[17]

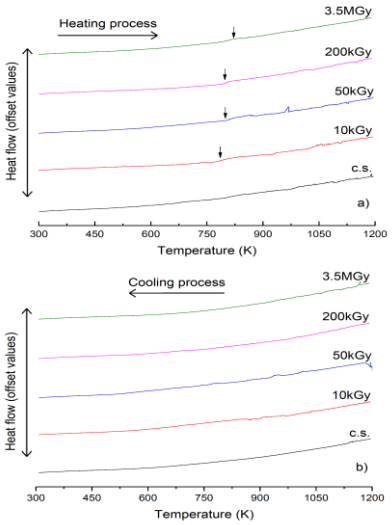

Figure 16. Temperature dependence of heat flow for nanocrystalline TiN particles: results corresponding to the heating (a) and cooling (b) processes.

[17] Huseynov, E.M., Hakhiyeva, R.R. Investigation of gamma irradiated nanocrystalline titanium carbide particles using thermal methods // *J Radioanal Nucl Chem*, – 2023, 332, – p. 3779–3785.

This observation shows that gamma irradiation modifies the surface properties of nanocrystalline TiN, effectively stabilizing it and making it less sensitive to thermal decomposition in the given temperature interval. As the temperature rises within the 600–850 K range, a noticeable mass increase is observed. This increase is explained by the onset of oxidation, as oxygen from the surrounding atmosphere begins to penetrate into the TiN nanoparticles.

At this stage, the formation of titanium dioxide (TiO_2) begins on the particle surface, and as the temperature approaches 850 K, the process becomes more pronounced. At approximately 850 K, oxidation can be considered nearly complete, since additional mass gain at higher temperatures is minimal.

These deviations indicate an exothermic reaction associated with the oxidation of TiN; the heat released by the reaction contributes to the overall heat flow. The increase in heat flow within this temperature interval is primarily attributed to the irradiation-induced enhancement of reactivity. Gamma irradiation creates additional defects and active sites on the TiN surface, thereby accelerating oxidation compared to unirradiated samples.

In contrast, during the cooling process shown in Figure 16b, no corresponding deviations in heat flow are observed, further confirming that oxidation predominantly occurs during the heating stage. The absence of significant changes in heat flow during cooling indicates that, after the oxidation reaction is completed, no additional major thermal transitions or reactions occur in the material, and the system maintains its thermal stability. [18]

MAIN SCIENTIFIC RESULTS

1. No phase transition is observed in TiN nanocrystals after gamma irradiation in the dose range of 50-3500 kGy. However, a decrease in the lattice parameter, a decrease in the average crystallite size of ~7.58%, and a decrease in the long-range order of ~2.51% at the highest dose were recorded.

[18] Chen, H.Y., Lu, F.H. Oxidation behavior of titanium nitride films // *J. Vac. Sci. Technol. A*, – 2005, 23, – p. 1006–1009.

2. It was found from PALS/DBAS experiments that with increasing irradiation dose, small volume defects transform into larger voids with a more homogeneous distribution in depth. In the Raman spectra, radiation dose-sensitive peak shifts and half-width changes were observed, especially in the mode corresponding to ~359 cm^{-1}.

3. From the DSC/TGA/DTA spectra, a temperature and a small mass change were recorded in the range of 740–800 K, which is justified by the formation of a new phase.

4. After annealing, a decrease in microstrain and an increase in the average size of nanoparticles up to ~50 nm were found at high irradiation doses. The decrease in the positron capture rate kd from 0.720 nm^{-1} to 0.709 nm^{-1} in PALS measurements is evidence of the shrinkage of large clusters. DBAS results showed that large vacancy clusters recombine at depths under the influence of temperature and defects migrate towards the particle boundaries.

5. After irradiation, the (Fm-3m) phase remained stable during annealing at 1173 K for 9 hours. XRD results showed that TiO_2 (rutile) is formed only on the surface and its fraction decreases from 6.4% to 3.88% with increasing irradiation dose. Thus, under the sequential action of gamma irradiation and annealing, TiN remains stable as a phase group, with only minor oxidation occurring on the surface. These results indicate that TiN is promising as a protective coating in high temperature and radiation environments.

SCIENTIFIC PUBLICATIONS ON THE DISSERTATION TOPIC

1. Abiyev, A.S., Huseynov, E.M., Hashimov, R.F. Gamma radiation-induced alterations in nanocrystalline titanium nitride (TiN) particles: a structural perspective // Radiation Physics and Chemistry, – 2024, 218, 111638.
2. Abiyev, A.S. Samadov, S. F., Mirzayev, M. N., Huseynov, E. M., Sidorin, A. A., Orlov, O. S., Popov, E. P. Defect formation analysis in gamma-irradiated titanium nitride nanocrystals: predictions from positron annihilation studies // Journal of Nanoparticle Research, - 2024, 26(7), 156.
3. Abiyev, A.S. Huseynov, E. M., Mirzayev, M. N., Mauyey, B., & Samadov, S. F. Positron annihilation lifetime and doppler broadening spectroscopies studies of defects in nano TiN crystal under gamma irradiation and high temperature // Indian Journal of Physics, – 2024, 98, – p. 4703-4709.
4. Abiyev, A.S. Samadov, S. F., Mehdiyeva, R. N., Dadashzade, G. A., Kvasovich, E. O., Huseynov, E. M. Oxidation dynamics in gamma-irradiated TiN nanoparticles after annealing // Ceramics International, - 2025, vol.51, - p. 28043-28048.
5. Abiyev A.S. Huseynov E. M. Investigating gamma radiation-induced modifications in titanium nitride (TiN) nanocrystals using DSC spectroscopy // Radiation Physics and Chemistry, - 2025, 232, 112652.
6. Abiyev A. S., Huseynov E.M. The Effects of Gamma Irradiation on TiN Nanocrystals // Курчатовский институт “OpenScience” - Санкт-Петербург, Россия: -15-17 november - 2023. – p. 57
7. Abiyev A. S., Samadov S., Huseynov E., Sidorin A.A., Orlov O.S. Qamma şüaların təsirinə məruz qalmış nanoölçülü TiN kristallarında defekt əmələgəlmə mexanizminin tədqiqi // Radiasiya təhlükəsizliyi problemləri: Regional aspektlər, Azərbaycan, Naxçıvan: – 18–19 oktyabr, – 2023, –p.95.
8. Abiyev A. S., Turchenko V.A., Huseynov E.M., Changes in crystallinity properties of TiN nanoparticles after gamma rays and long – term heating process // II International Conference

‘Fundamental and Applied Problems of Semiconductor Physics, Micro- and Nanoelectronics - Tashkent, Uzbekistan: - 2023, - p. 261-262.
9. Abiyev A. S., Samadov S.F., Huseynov E.M. Defect formation analysis in gamma-irradiated titanium nitride nanocrystals:predictions from positron annhilation studies // Metal və ərintilər fizikasının aktual problemləri” Respublika Elmi-Praktiki Konfransı - Azərbaycan. -2025, -p.146-148.
10. Abiyev A. S., Huseynov E.M. Characterization of Thermal Effects on TiN Nanocrystals after Gamma Irradiation // Молодежная Школа по физике конденсированного состояния (Школа ФКС-2025) - Рощино, Ленинградская область: - 24 - 28 марта 2025, p.134.
11. Abiyev, A.S., Huseynov, E.M., Aliyev, Y.I., Asadov, A.G., Sobirjonov, A.K., Huseynov, H.J., Guliyeva, K.M., Effect of ionizing gamma radiation on vibrational properties of TiN nanoparticles // Radiation Physics and Chemistry. 113330. https://doi.org/10.1016/j.radphyschem.2025.113330

The defense will be held 30 october 2025, at 11:00 the meeting of the FD1.21 Dissertation Council operating under the Institute of Radiation Problems of the Ministry of Science and Education of the Republic of Azerbaijan.

Address: AZ 1143, Baku, B. Vahabzadeh Street, 9.

The dissertation is available for review in the scientific library of the Institute of Radiation Problems of the Ministry of Science and Education of the Republic of Azerbaijan.

Electronic versions of the dissertation and abstract are posted on the official website of the Institute of Radiation Problems of the Ministry of Science and Education of the Republic of Azerbaijan.

The abstract was sent to the necessary addresses on «29» september 2025.

Signed to print: 26.09.2025

Paper formatı: A5

Volume: 39 034

Circulation: 20